Performance Analysis of Recoverable Flight Control Systems Using Hybrid Dynamical Models

Hong Zhang, W. Steven Gray and Oscar R. González

Abstract— The main goal of this paper is to describe and *validate* a specific hybrid dynamical model for NASA's Recoverable Computer System subjected to simulated random upsets. The system is in closed-loop with a Boeing 737 simulation model which is flying at cruising altitude. The validation is based on a controlled experiment where the computer upsets are injected into the system at a desired rate, and the effects on the output tracking performance of a simulated aircraft are directly observed and quantified. The hybrid model consists of a jump-linear system driven by a finite-state machine with a Markov input. The jump-linear system models the switched dynamics of the closed-loop due to the presence of controller recoveries, the finite-state machine models the recovery logic, and the Markov input acts as an upset generator. Stability analysis is performed on the hybrid model using existing techniques. The paper supplies the additional performance theory for analyzing the tracking error mean output power. The results are compared against experimental data, showing good agreement.

I. INTRODUCTION

It has been observed that atmospheric neutrons can produce single-event upsets (SEU's) in digital flight control hardware [1]–[4]. SEU's are soft faults, which are usually transient and nondestructive to the hardware. But if a sequence of bit errors is not detected and corrected, it can cause system errors and reduce closed-loop performance. Different error recovery mechanisms have been considered for restoring the controller back to its nominal state. One experimental approach is NASA Langley Research Center's Recoverable Computer System (RCS). Developed by Honeywell, Inc., the system implements its error recovery using dual-lock-step processors together with new fault-tolerant architectures and communication subsystems [5], [6]. It employs a variation of rollback recovery [7], [8] via the following steps: checkpointing, fault-tolerant comparison, rollback, and retry. During a checkpoint, the state of each microprocessor module is stored. When an upset is detected, rollback of both microprocessor modules to a previous checkpoint takes place, and then the system is allowed to proceed with normal execution. But during rollback, the execution of the normal control program is interrupted, and the execution of a different control law takes place, one that has significantly different dynamics and is on a time scale that can alter the overall closed-loop dynamics of the flight control system. Therefore, the two control modes for this system are the nominal mode and the recovery mode. A conceptual diagram of the RCS in a closed-loop configuration is shown in Fig. 1.

In [9], a general Markov jump-linear model was developed for predicting output tracking error caused by neutron-induced upsets to a generic recoverable control computer. In this paper, the main goal is to fully describe
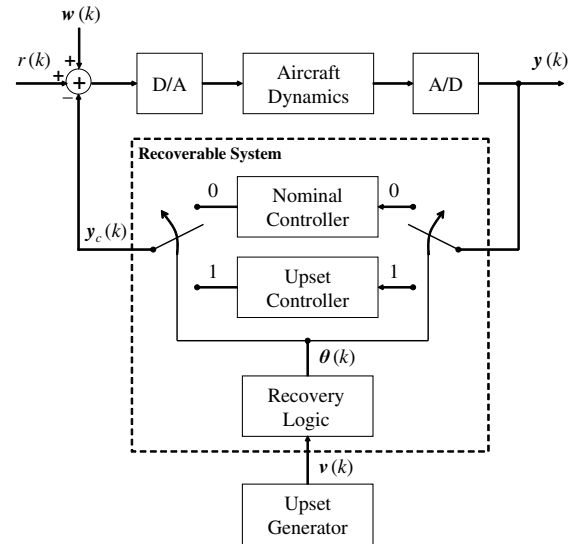
Fig. 1. A conceptual closed-loop flight control system with a recoverable flight control computer.

and *validate* a specific hybrid dynamical model for NASA's RCS when subjected to random upsets and in closed-loop with a Boeing 737 at cruising altitude. The validation is based on a controlled experiment where the computer upsets are injected into the system at a desired rate, and the effects on the output tracking performance of a simulated aircraft are directly observed and quantified. In an actual neutron experiment, the upset rate cannot be precisely observed or controlled, so this current experiment is viewed as a precursor where the models and the theory can be tested. The hybrid model shown in Fig. 2 consists of a jump-linear system driven by a finite-state machine (FSM) with a Markov input. The jump-linear system models the
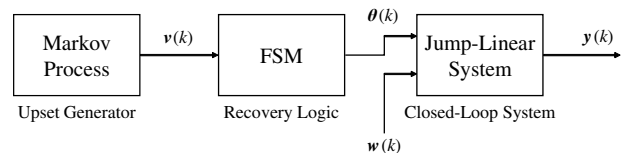
Fig. 2. The hybrid model for the closed-loop system with a recoverable flight control computer when $r(k) \equiv 0$.

switched dynamics of the closed-loop due to the presence of controller recoveries, the FSM approximately models the recovery logic, and the Markov input acts as the upset generator. Stability analysis is performed on the hybrid model using the results in [10], [11]. This paper supplies the additional theory required to do the tracking error performance predictions. The results are compared against experimental data, showing good agreement.

The paper is organized as follows. Section II gives a brief description of the two experiments used to test the RCS's tracking performance. Section III describes how to model and calculate the tracking error theoretically. Section IV applies the results obtained in Section III to the analysis of the real RCS system.

The mathematical notation used throughout this paper is largely consistent with [9], [12]. The symbol $\mathbb{Z}^+$ denotes the set of all non-negative integers. $\mathbb{R}^n$ is the n-dimensional real vector space, and $\mathbb{M}(\mathbb{R}^n)$ is the normed linear space of all $n \times n$ real matrices. The subset of all symmetric positive semi-definite matrices is $\mathbb{M}(\mathbb{R}^n)^+$. $\mathbb{H}^n = \{V = (V_1, V_2 \ldots, V_N) : V_i \in \mathbb{M}(\mathbb{R}^n)\}$ will be used to denote the space of all N-tuples of $n \times n$ real matrices. If every V_i of a given V in $\mathbb{H}^n$ is positive definite or positive semi-definite, this is indicated, respectively, by $V > 0$ and $V \geq 0$. $\mathbb{H}^{n+}$ denotes the set $\{V \in \mathbb{H}^n : V \geq 0\}$. Given $U, V \in \mathbb{H}^n$, the inner product on $\mathbb{H}^n$ is defined by

$$\langle U, V \rangle = \sum_{i=1}^{N} \operatorname{tr}\left(U_i^{\mathrm{T}} V_i\right),$$

and $\|V\|^2 = \langle V, V \rangle$ is the induced norm squared of V. ($\| \cdot \|$ will also be used for representing the standard norm on $\mathbb{R}^n$.) $\mathbb{B}(\mathbb{H}^n)$ is the space of all bounded linear operators on $\mathbb{H}^n$ under the induced operator norm

$$\|\mathcal{L}\| = \sup_{V \neq 0} \frac{\|\mathcal{L}(V)\|}{\|V\|},$$

where $\mathcal{L} \in \mathbb{B}(\mathbb{H}^n)$. $r_\sigma(\mathcal{L})$ is used to denote the spectral radius of $\mathcal{L}$, specifically, $r_\sigma(\mathcal{L}) = \|\mathcal{L}\|$.

II. Two Experiments for Testing the RCS Performance

Two experiments have been done to assess the performance of the RCS: one in a simulated neutron environment and the other in a real neutron environment. The first experiment was conducted at the NASA Langley Research Center's SAFETI Laboratory. The RCS flight control system was connected in closed-loop with a Boeing 737 flight simulation system running on a separate host computer. The input reference signals were set to maintain straight and level flight at a cruising altitude of $34,000$ feet. A data acquisition system was maintained on a third computer system. It collected flight data during the simulation. Neutron interactions were simulated by manually triggering rollback recoveries according to a pre-determined Markov upset process while the aircraft flew in 1 ft/sec (light) winds. High wind conditions were not tested since in general, they can excite nonlinear modes in the aircraft dynamics, which are not modeled in the present jump-linear framework. Data was collected for 60 one-hour sample flights. The aircraft's state variables were compared against nominal flights, i.e., ones with no rollback recoveries but with identical wind conditions. The tracking error statistics were then computed.

The second experiment was done at the Los Alamos Neutron Science Center (LANSCE) in Los Alamos, New Mexico. A conceptual diagram of the testbed for the LANSCE experiments is shown in Fig. 3. A beam of free neutrons was directed through a flux sensor at the device under test, in this case the RCS. The energy spectrum of the
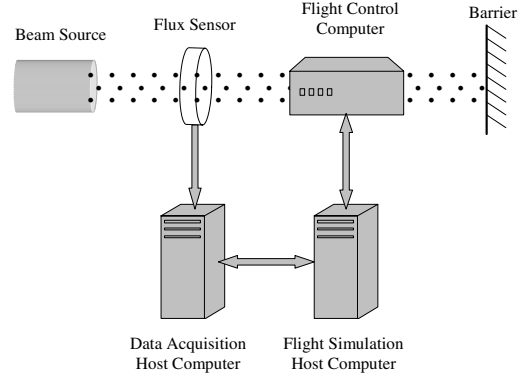
Fig. 3. The testbed for the LANSCE experiments [9].

neutron source has a very similar shape to that produced by atmospheric neutrons albeit at a flux density approximately 10^6 times higher than real atmospheric conditions. The method of data collection was similar to that done in the NASA experiments. In this paper, our focus is on validating the performance modeling using data from the simulated neutron experiment. Future publications will address the LANSCE experiment.

III. Theory for Calculating Tracking Error Performance

A. The Output Tracking Error System

The closed-loop dynamics of the flight control system with an RCS can be modeled as a jump-linear system with two modes: the nominal mode and the recovery mode. In general, the system operates in the nominal mode. However, when a neutron encounter produces a detectable SEU in the flight control hardware, the RCS will rollback the state of the controller to its stored value at the previous checkpoint. During this recovery process, the current control output values are frozen until the checkpointed values can be reloaded and made available. During this process, the system is said to be in recovery mode. Let the reference input $r(k) \equiv 0$. When compared against the nominal (unswitched) system, the jump-linear system gives rise to an output tracking error described by the following state space model:

$$\boldsymbol{x}_e(k+1) = A_{e,\boldsymbol{\theta}(k)}\,\boldsymbol{x}_e(k) + G_{e,\boldsymbol{\theta}(k)}\boldsymbol{w}(k), \quad (1a)$$
$$\boldsymbol{x}_e(0) = \boldsymbol{x}_{e,0}, \quad \boldsymbol{\theta}(0) = \boldsymbol{\theta}_0$$
$$\boldsymbol{y}_e(k) = C_{e,\boldsymbol{\theta}(k)}\boldsymbol{x}_e(k), \quad (1b)$$

where $\boldsymbol{x}_e(k) = \begin{bmatrix} \tilde{\boldsymbol{x}}^{\mathrm{T}}(k) & \tilde{\boldsymbol{x}}_n^{\mathrm{T}}(k) \end{bmatrix}^{\mathrm{T}}$, $A_{e,\boldsymbol{\theta}(k)} = \operatorname{diag}\left(\tilde{A}_{\boldsymbol{\theta}(k)}, \tilde{A}_n\right)$, $G_{e,\boldsymbol{\theta}(k)} = \begin{bmatrix} \tilde{G}_{\boldsymbol{\theta}(k)}^{\mathrm{T}} & \tilde{G}_n^{\mathrm{T}} \end{bmatrix}^{\mathrm{T}}$ and $C_{e,\boldsymbol{\theta}(k)} = \begin{bmatrix} \tilde{C}_{\boldsymbol{\theta}(k)} & -\tilde{C}_n \end{bmatrix}$. The random process $\boldsymbol{\theta}(k)$ switches between the symbols "n" and "r" representing the "nominal" mode and the "recovery" mode, respectively; $\tilde{\boldsymbol{x}}(k)$ and $\tilde{\boldsymbol{x}}_n(k)$ are the state vectors of the switched and nominal closed-loop systems; $\boldsymbol{w}(k)$ is a zero-mean white noise process used to generate a wind input; and $\boldsymbol{y}_e(k)$ is the closed-loop output tracking error.

The system is always assumed to be stochastically stable in the following sense.

Definition 1: [13] System (1a) with $\boldsymbol{w}(k) = 0$ is mean-square stable (MSS) if $E\left\{\|\boldsymbol{x}_e(k)\|^2\right\} \to 0$ as $k \to \infty$ for any initial condition $\boldsymbol{x}_{e,0}$ with a finite second-order moment and any initial distribution for $\boldsymbol{\theta}_0$.

In addition, it was shown in [9] that if system (1a) is MSS, and if winds and gusts are present, i.e., $\boldsymbol{w}(k) \neq 0$, then $\boldsymbol{y}_e(k)$ has finite average power

$$J_w := \lim_{k \to \infty} E\left\{\|\boldsymbol{y}_e(k)\|^2\right\}.$$

An analytical calculation for J_w was given in [9] for a linear system described by $\tilde{\Sigma}_{\boldsymbol{\theta}(k)} : \left(A_{\boldsymbol{\theta}(k)}, G, C_{\boldsymbol{\theta}(k)}\right)$, where the noise input matrix G was non-switching. In the next subsection, an extended method for calculating the average power is given for the case where G is switched. This result is needed in the subsequent sections.

B. Calculating the Mean Output Power

Consider the following stochastic system over a probability space $(\Omega, \mathcal{F}, \text{Pr})$

$$\boldsymbol{x}(k+1) = A_{\boldsymbol{\theta}(k)}\boldsymbol{x}(k) + G_{\boldsymbol{\theta}(k)}\boldsymbol{w}(k), \quad (2a)$$
$$\boldsymbol{x}(0) = \boldsymbol{x}_0, \quad \boldsymbol{\theta}(0) = \boldsymbol{\theta}_0$$
$$\boldsymbol{y}(k) = C_{\boldsymbol{\theta}(k)}\boldsymbol{x}(k), \quad (2b)$$

where $\boldsymbol{x}_0$ is a second-order random variable; $\{\boldsymbol{w}(k); k \in \mathbb{Z}^+\}$ is a stationary zero mean white noise process with covariance matrix I_m, independent of $\boldsymbol{x}_0$ and $\boldsymbol{\theta}(k)$; $\{\boldsymbol{\theta}(k); k \in \mathbb{Z}^+\}$ is an aperiodic, ergodic Markov chain with states $\{1, 2, \ldots, N\}$ and transition probability matrix $\Pi = [\pi_{ij}]$. If $\boldsymbol{\theta}_s$ is a random variable with the same distribution as the unique stationary distribution of $\boldsymbol{\theta}(k)$, then $\pi(i) := \text{Pr}\{\boldsymbol{\theta}_s = i\}$ is determined by solving the eigenequation

$$\begin{bmatrix} \pi(1) \\ \vdots \\ \pi(N) \end{bmatrix} = \Pi^{\mathrm{T}} \cdot \begin{bmatrix} \pi(1) \\ \vdots \\ \pi(N) \end{bmatrix}.$$

Let $A = (A_1, A_2, \ldots, A_N) \in \mathbb{H}^n$, $\bar{C} = \left(C_1^{\mathrm{T}}C_1, C_2^{\mathrm{T}}C_2, \ldots, C_N^{\mathrm{T}}C_N\right) \in \mathbb{H}^{n+}$ and $\bar{G} = \left(G_1 G_1^{\mathrm{T}}, G_2 G_2^{\mathrm{T}}, \ldots, G_N G_N^{\mathrm{T}}\right) \in \mathbb{H}^{n+}$. For any $S = (S_1, S_2, \ldots, S_N) \in \mathbb{H}^n$, define an operator $\mathcal{E} \in \mathbb{B}(\mathbb{H}^n)$ by $\mathcal{E}(S) = \left(\mathcal{E}_1(S), \mathcal{E}_2(S), \ldots, \mathcal{E}_N(S)\right)$, where

$$\mathcal{E}_i(S) = \sum_{j=1}^{N} \pi_{ij} S_j.$$

Similarly, define the operator $\mathcal{L} \in \mathbb{B}(\mathbb{H}^n)$ by $\mathcal{L}(S) = \left(\mathcal{L}_1(S), \mathcal{L}_2(S), \ldots, \mathcal{L}_N(S)\right)$, where $\mathcal{L}_i(S) = A_i^{\mathrm{T}}\mathcal{E}_i(S)A_i$. The matrix representation of $\mathcal{L}$ is

$$\mathscr{A}_2 := \text{diag}\left(A_1^{\mathrm{T}} \otimes A_1^{\mathrm{T}}, \ldots, A_N^{\mathrm{T}} \otimes A_N^{\mathrm{T}}\right) \cdot (\Pi \otimes I_{n^2}),$$

where $\otimes$ denotes the Kronecker product. In [12] it is shown that system (2) is MSS if and only if $r_\sigma(\mathcal{L}) = r_\sigma(\mathscr{A}_2) < 1$. For $Q = (Q_1, Q_2, \ldots, Q_N) \in \mathbb{H}^n$, where $Q_i = \begin{bmatrix} q_{i1} & q_{i2} & \cdots & q_{in} \end{bmatrix}$, and $q_{ij} \in \mathbb{R}^n$ for $i = 1, 2, \ldots, N$ and $j = 1, 2, \ldots, n$, define the operators vec and φ on $\mathbb{M}(\mathbb{R}^n)$ and $\mathbb{H}^n$, respectively, such that $\text{vec}(Q_i) = \begin{bmatrix} q_{i1}^{\mathrm{T}} & q_{i2}^{\mathrm{T}} & \cdots & q_{in}^{\mathrm{T}} \end{bmatrix}^{\mathrm{T}}$ is the column stack of Q_i and $\varphi(Q) = \begin{bmatrix} \text{vec}^{\mathrm{T}}(Q_1) & \text{vec}^{\mathrm{T}}(Q_2) & \cdots & \text{vec}^{\mathrm{T}}(Q_N) \end{bmatrix}^{\mathrm{T}} \in \mathbb{R}^{Nn^2}$.

vec^{-1} and φ^{-1} are used to denote their corresponding inverse operators. The following theorem is a variation of Proposition 8 in [14].

Theorem 1: For an MSS system (2), where $\boldsymbol{\theta}(k)$ is aperiodic and ergodic, let $\bar{Q}_i(k) := E\left\{\boldsymbol{x}_i(k)\boldsymbol{x}_i^{\mathrm{T}}(k) \cdot \boldsymbol{1}_{\{\boldsymbol{\theta}(k)=i\}}\right\}$ for any $k \in \mathbb{Z}^+$ and $\bar{Q}_i := \lim_{k \to \infty} \bar{Q}_i(k)$. If $\boldsymbol{x}_0$, $\boldsymbol{w}$, and $\boldsymbol{\theta}$ are independent then

$$\bar{Q}_i = \varphi_i^{-1}\left(\left(I_{Nn^2} - \mathscr{A}_1\right)^{-1}\varphi\left(V_1, \ldots, V_N\right)\right),$$

where $V_j := \sum_{i=1}^{N} \pi_{ij}G_iG_i^{\mathrm{T}}\pi(i)$ and $\mathscr{A}_1 := \mathscr{A}_2^{\mathrm{T}}$.

Corollary 1: For an MSS system (2), where $\boldsymbol{\theta}(k)$ is aperiodic and ergodic, if $\boldsymbol{x}_0 = 0$, and $\boldsymbol{w}$ and $\boldsymbol{\theta}$ are assumed to be independent then

$$J_w = \text{tr}\left(\sum_{j=1}^{N}\left[\bar{C}_j\bar{Q}_j\right]\right). \quad (3)$$

The main result of this section is given in the following theorem.

Theorem 2: For an MSS system (2), where $\boldsymbol{\theta}(k)$ is aperiodic and ergodic, if $\boldsymbol{x}_0 = 0$, and $\boldsymbol{w}$ and $\boldsymbol{\theta}$ are assumed to be independent then

$$J_w = \lim_{k \to \infty} E\left\{\text{tr}\left(\sum_{i=0}^{k-1}\left[G_{\boldsymbol{\theta}(k-i-1)}^{\mathrm{T}}\mathcal{L}_{\boldsymbol{\theta}(k-i)}^{i}(\bar{C})G_{\boldsymbol{\theta}(k-i-1)}\right]\right)\right\}$$
$$= \text{tr}\left(E\left\{G_{\boldsymbol{\theta}_s}^{\mathrm{T}}\mathcal{E}_{\boldsymbol{\theta}_s}\left(\sum_{k=0}^{\infty}\mathcal{L}^k(\bar{C})\right)G_{\boldsymbol{\theta}_s}\right\}\right)$$
$$= \text{tr}\left(E\left\{\bar{G}_{\boldsymbol{\theta}_s}\tilde{Q}_{\boldsymbol{\theta}_s}\right\}\right), \quad (4)$$

where $\bar{G}_{\boldsymbol{\theta}_s} := G_{\boldsymbol{\theta}_s}G_{\boldsymbol{\theta}_s}^{\mathrm{T}}$ and $\tilde{Q}_{\boldsymbol{\theta}_s} := \mathcal{E}_{\boldsymbol{\theta}_s}\left(\sum_{k=0}^{\infty}\mathcal{L}^k(\bar{C})\right)$.

Proof: It will be shown that (3) and (4) are equivalent. Let $Q = (Q_1, Q_2, \ldots, Q_N) := \sum_{i=0}^{\infty}\mathcal{L}_i(\bar{C})$ then

$$\varphi(Q) = \left(I_{Nn^2} - \mathscr{A}_2\right)^{-1}\begin{bmatrix} C_1^{\mathrm{T}} \otimes C_1^{\mathrm{T}} \\ \vdots \\ C_N^{\mathrm{T}} \otimes C_N^{\mathrm{T}} \end{bmatrix}\text{vec}(I_p),$$

and

$$\tilde{Q}_i = \mathcal{E}_i(Q) = \sum_{j=1}^{N}\pi_{ij}Q_j$$
$$= \begin{bmatrix} Q_1 & \cdots & Q_N \end{bmatrix}\left(\begin{bmatrix} \pi_{i1} \\ \vdots \\ \pi_{iN} \end{bmatrix} \otimes I_n\right).$$

A direct calculation shows that

$$\text{tr}\left(G_{\boldsymbol{\theta}_s}^{\mathrm{T}}\mathcal{E}_{\boldsymbol{\theta}_s}(Q)G_{\boldsymbol{\theta}_s}\right) = \text{tr}\left(\text{vec}^{-1}\left(M\,\text{vec}(I_p)\right)\right), \quad (5)$$

where

$$M := \begin{bmatrix} \sum_{i=1}^{N}\pi_{i1}\pi(i)G_i^{\mathrm{T}} \otimes G_i^{\mathrm{T}} & \cdots & \sum_{i=1}^{N}\pi_{iN}\pi(i)G_i^{\mathrm{T}} \otimes G_i^{\mathrm{T}} \end{bmatrix}$$
$$\cdot \left(I_{Nn^2} - \mathscr{A}_2\right)^{-1}\begin{bmatrix} C_1^{\mathrm{T}} \otimes C_1^{\mathrm{T}} \\ \vdots \\ C_N^{\mathrm{T}} \otimes C_N^{\mathrm{T}} \end{bmatrix}.$$

Next observe that according to Theorem 1, if $V_j := \sum_{i=1}^{N} \pi_{ij} G_i G_i^{\mathrm{T}} \pi(i)$ for $j \in \{1, 2, \ldots, N\}$, then for $V = (V_1, V_2, \ldots, V_N)$,

$$\varphi(V) = \begin{bmatrix} \mathrm{vec}(V_1) \\ \vdots \\ \mathrm{vec}(V_N) \end{bmatrix} = \begin{bmatrix} \sum_{i=1}^{N} \pi_{i1} \pi(i) G_i \otimes G_i \\ \vdots \\ \sum_{i=1}^{N} \pi_{iN} \pi(i) G_i \otimes G_i \end{bmatrix} \mathrm{vec}(I_m).$$

Therefore,

$$\varphi(\bar{Q}) = (I_{Nn^2} - \mathscr{A}_1)^{-1} \varphi(V)$$

$$= (I_{Nn^2} - \mathscr{A}_1)^{-1} \begin{bmatrix} \sum_{i=1}^{N} \pi_{i1} \pi(i) G_i \otimes G_i \\ \vdots \\ \sum_{i=1}^{N} \pi_{iN} \pi(i) G_i \otimes G_i \end{bmatrix} \mathrm{vec}(I_m).$$

But according to Corollary 1,

$$J_w = \mathrm{tr}\left(\sum_{i=1}^{N} [C_j \bar{Q}_j C_j^{\mathrm{T}}] \right)$$

$$= \mathrm{tr}\left(\mathrm{vec}^{-1}\left([C_1 \otimes C_1 \quad \cdots \quad C_N \otimes C_N] \varphi(\bar{Q}) \right) \right)$$

$$= \mathrm{tr}\left(\mathrm{vec}^{-1}\left([C_1 \otimes C_1 \quad \cdots \quad C_N \otimes C_N] \right.\right.$$

$$\left.\left. \cdot (I_{Nn^2} - \mathscr{A}_1)^{-1} \begin{bmatrix} \sum_{i=1}^{N} \pi_{i1} \pi(i) G_i \otimes G_i \\ \vdots \\ \sum_{i=1}^{N} \pi_{iN} \pi(i) G_i \otimes G_i \end{bmatrix} \mathrm{vec}(I_m) \right) \right)$$

$$= \mathrm{tr}\left(\mathrm{vec}^{-1}\left(M^{\mathrm{T}} \mathrm{vec}(I_m) \right) \right). \tag{6}$$

It is easy to prove that the right-hand sides of (5) and (6) are equivalent, thus the proof is complete. ∎

When system (2) is MSS, J_w can be calculated numerically as follows. It is clear that $Q = \sum_{k=0}^{\infty} \mathcal{L}^k(\bar{C})$ is the unique solution to the adjoint coupled Lyapunov equation $Q - \mathcal{L}(Q) = \bar{C}$ (the observability Gramian in [12]), which can be solved using $\mathscr{A}_2$ (see [12], [14] for details). Using φ, the equation can be written as the matrix equation $\varphi(Q) - \mathscr{A}_2 \cdot \varphi(Q) = \varphi(\bar{C})$, and hence $Q = \varphi^{-1}\left((I_{Nn^2} - \mathscr{A}_2)^{-1} \cdot \varphi(\bar{C}) \right)$. Therefore,

$$J_w = \mathrm{tr}\left(E\left\{ \bar{G}_{\boldsymbol{\theta}_s} \tilde{Q}_{\boldsymbol{\theta}_s} \right\} \right) = \mathrm{tr}\left(\sum_{i=1}^{N} \left(\bar{G}_i \tilde{Q}_i \cdot \pi(i) \right) \right).$$

The following corollary shows that Theorem 4.2(b) in [9] is a special case of Theorem 2.

Corollary 2: In the context of Theorem 2, if $G_i = G$ for $i = 1, 2, \ldots, N$ then

$$J_w = \mathrm{tr}\left(G_w E\left\{ \tilde{Q}_{\boldsymbol{\theta}_s} \right\} \right) \equiv \mathrm{tr}(G_w Q_w),$$

where $G_w := GG^{\mathrm{T}}$ and $Q_w := E\{Q_{\boldsymbol{\theta}_s}\}$.

Corollary 3: If $N = 1$, then system (2) is a non-switching system. Let $A_1 = \hat{A}$ with $r_\sigma\left(\hat{A}\right) < 1$, $G_1 = G$ and $C_1 = C$. Then $J_w = \mathrm{tr}\left(G_w \hat{Q}_w\right)$, where $G_w := GG^{\mathrm{T}}$ and $\hat{Q}_w := \sum_{k=0}^{\infty} \left[\left(\hat{A}^{\mathrm{T}}\right)^k C^{\mathrm{T}} C \hat{A}^k \right]$, which is exactly the observability Gramian matrix.

IV. Modeling and Performance Analysis of the Boeing 737 Model with an RCS

A. System Identification of the Boeing 737 Simulation Model with an RCS

The first step in the model building process was to identify two state space models for the Boeing 737 in level flight: one for the nominal mode $\Sigma_n : (A_n, G_n, C_n)$ and one for the recovery mode $\Sigma_r : (A_r, G_r, C_r)$. Input/output (I/O) data was collected for identification using the nonlinear Boeing 737 Simulink model described in [15]. The control characteristics of the RCS are discussed in [16], [17]. From (1), it is clear that the only "inputs" in this case are the noises, which are used in the Simulink code to drive the Dryden wind gusts model. The output signals were the altitude of the aircraft, the calibrated airspeed, and the track angle. The function pem from MATLAB's System Identification Toolbox was used for identifying the models. Seventeen sets of data containing 2,000 samples each were used for building the nominal model, and another 35 sets of data were used to verify the model. The identified model for the nominal mode Σ_n was an eighth-order system. Similarly, because the recovery mode is usually unstable, it is assumed that the system normally operates in this mode for a short period of time. Therefore, 190 data sets with 200 samples per set were used to identify the recovery model. Another 35 sets were used for verification. The identified model of the recovery mode Σ_r was sixth-order.

B. The Switched System

It is only possible to switch between Σ_n and Σ_r if their respective state space coordinate systems are the same. But here not even their dimensions are equivalent. To remedy the situation, Σ_r was embedded into an eighth-order system in such a way that the new system, $\tilde{\Sigma}_r$, has the same controllability indices as Σ_n, specifically, $\{3, 3, 2\}$. Therefore, each system can be transformed to the same Brunovsky form, and the switching can be done (formally) by simply switching between state space gain matrices, $\tilde{K}_n$ and $\tilde{K}_r$, and input transformation matrices, $\tilde{L}_n$ and $\tilde{L}_r$. Specifically, Fig. 4 shows how the Brunovsky canonical form acts as a "bridge" between the controller canonical forms of the two modes. Σ_n is transformed into its controller canonical form $\tilde{\Sigma}_n$ by T_n. Σ_r is transformed into its controller canonical form $\tilde{\Sigma}_r : (\bar{A}_r, \bar{G}_r, \bar{C}_r)$ by T_r, then two stable states are added to $\bar{\Sigma}_r$ to produce an eighth-order system $\tilde{\Sigma}_r$. Now $\tilde{\Sigma}_n$ and $\tilde{\Sigma}_r$ can be transformed to the same Brunovsky canonical form (A°, G°) by $\left(\tilde{K}_n, \tilde{L}_n\right)$ and $\left(\tilde{K}_r, \tilde{L}_r\right)$, respectively, since $A^\circ = \tilde{A}_n - \tilde{G}_n \tilde{L}_n \tilde{K}_n = \tilde{A}_r - \tilde{G}_r \tilde{L}_r \tilde{K}_r$ and $G^\circ = \tilde{G}_n \tilde{L}_n = \tilde{G}_r \tilde{L}_r$. The switching between $\tilde{\Sigma}_n$ and $\tilde{\Sigma}_r$ can be done using $\tilde{K} := \tilde{K}_n - \tilde{K}_r$, $\tilde{L}_n$ and $\tilde{L}_r$, because $\tilde{A}_n = \tilde{A}_r + G^\circ \tilde{K}$ and $\tilde{G}_n = \tilde{G}_r \tilde{L}_r \tilde{L}_n^{-1}$.
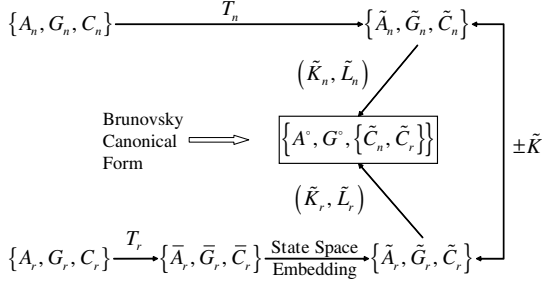
Fig. 4. The Brunovsky canonical form acts as a "bridge" between the state space models for the two system modes.

C. Rollback Recovery Process Modeling

The rollback recovery process can be modeled in a variety of ways. The most accurate approach models the actual freezing of the control signals, the rolling back of the control data, the logic of the recovery process, and the delay introduced into the feedback loop. Such an approach is described in [18], [19]. In this study, however, a much simpler approach was taken, only the rollback recovery delay is modeled. A series of experiments showed that over 80% of the recovery periods of the RCS were six frames in length. Any request for a recovery during an active recovery process was ignored. This information was encoded into the FSM shown in Fig. 5. The input process to the FSM
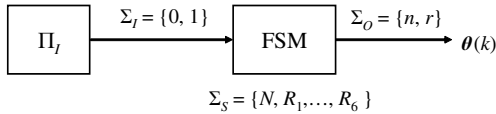
Fig. 5. The finite-state machine modeling the recovery process.

is a homogeneous, two-state, first-order Markov chain. The probability transition matrix of the Markov chain is Π_I. The set of states for the Markov chain is $\Sigma_I = \{0, 1\}$, where "0" indicates that no upset was detected and "1" indicates that an upset has been detected. This Markov chain then drives an FSM $\mathcal{M} = (\Sigma_I, \Sigma_S, \Sigma_O, \delta, \omega)$, where $\Sigma_S = \{N, R_1, \ldots, R_6\}$ is the set of the machine states, $\Sigma_O = \{n, r\}$ is the set of output symbols, $\delta : \Sigma_I \times \Sigma_S \to \Sigma_S$ is a next state mapping, and $\omega : \Sigma_S \to \Sigma_O$ is the output mapping. The FSM produces at its output the switching signal $\boldsymbol{\theta}(k)$. Fig. 6 shows the state diagram. When the FSM is in the nominal state N, and if the input is 0, the FSM will remain in the nominal state, else, it will transit to recovery mode R_1. If the FSM is in one of its six recovery states, R_i, then the input is ignored and the state will always transit to the next recovery state R_{i+1} when $i = 1, \ldots, 5$ or back to its nominal state N when $i = 6$. Let $e_j := [0 \quad \cdots \quad 0 \quad \underbrace{1}_{j\text{th}} \quad 0 \quad \cdots \quad 0]^{\mathrm{T}}$ for $j = 1, 2, \ldots, 7$. As described in [10], [11], S_0 and S_1 are the corresponding state transition matrices of the FSM shown in Fig. 6 for the input symbols 0 and 1, respectively:

$$S_0 = \begin{bmatrix} e_1^{\mathrm{T}} & e_3^{\mathrm{T}} & e_4^{\mathrm{T}} & e_5^{\mathrm{T}} & e_6^{\mathrm{T}} & e_7^{\mathrm{T}} & e_1^{\mathrm{T}} \end{bmatrix}^{\mathrm{T}},$$
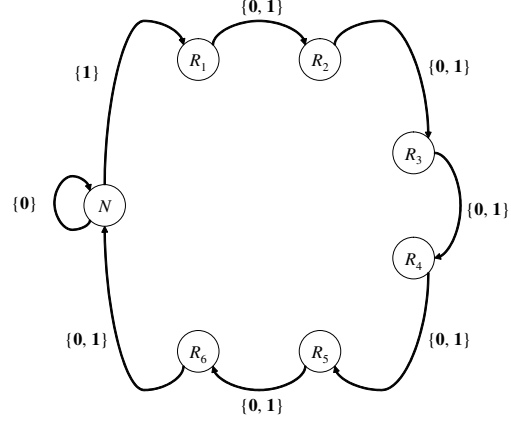
Fig. 6. The state diagram for the FSM.

and

$$S_1 = \begin{bmatrix} e_2^{\mathrm{T}} & e_3^{\mathrm{T}} & e_4^{\mathrm{T}} & e_5^{\mathrm{T}} & e_6^{\mathrm{T}} & e_7^{\mathrm{T}} & e_1^{\mathrm{T}} \end{bmatrix}^{\mathrm{T}}.$$

D. Stability Analysis of the Hybrid Dynamical System

It is known that the cross product of the input process and the output process is a Markov chain with transition matrix

$$\Pi_{I/O} = \operatorname{diag}(S_0, S_1) \cdot (\Pi_I \otimes I_7).$$

If the two-mode, 16th-order switched system with system matrices $\operatorname{diag}\left(\tilde{A}_n, \tilde{A}_n\right)$ and $\operatorname{diag}\left(\tilde{A}_r, \tilde{A}_n\right)$ is driven by this cross chain process, the mean-square stability of the hybrid system can be determined from the spectral radius of the following matrix according to [10], [11]:

$$\tilde{\mathscr{A}}_1 := \left(\Pi_{I/O}^{\mathrm{T}} \otimes I_{16^2}\right) \cdot \operatorname{diag}(A_{0,N} \otimes A_{0,N}, A_{0,R_1} \otimes A_{0,R_1},$$
$$\ldots, A_{0,R_6} \otimes A_{0,R_6}; A_{1,N} \otimes A_{1,N},$$
$$A_{1,R_1} \otimes A_{1,R_1}, \ldots, A_{1,R_6} \otimes A_{1,R_6}),$$

where $A_{j,N} \equiv \operatorname{diag}\left(\tilde{A}_n, \tilde{A}_n\right)$ and $A_{j,R_i} \equiv \operatorname{diag}\left(\tilde{A}_r, \tilde{A}_n\right)$ for $i = 1, 2, \ldots, 6$ and $j = 0, 1$. Now let $\Pi_I = \begin{pmatrix} 1 - \pi_{I,01} & \pi_{I,01} \\ 1 & 0 \end{pmatrix}$, where parameter $\pi_{I,01}$ is equivalent to the probability of an upset. Fig. 7 shows the spectral radius of $\tilde{\mathscr{A}}_1$ as a function of $\pi_{I,01}$ using the identified models. The hybrid system is MSS only when $\pi_{I,01} < 0.0015$.

E. Comparison Between Predicted and Actual Tracking Error Performance

Sixty one-hour real-time experiments were done at NASA Langley's SAFETI Lab. Ten sets of experimental data were collected for six upset probabilities ($\pi_{I,01}$): 0, 0.0001, 0.0004, 0.0006, 0.0009, and 0.0012. In each case, different sample functions from the corresponding Markov process $\boldsymbol{\nu}(k)$ were used to supply the RCS with a series of recovery requests for the closed-loop system. The ten experimental output powers of $\boldsymbol{y}_e(k)$ for each value of $\pi_{I,01}$ are shown in Fig. 8. There were only ten samples for each probability. Cluster analysis diagrams were used to exclude the outliers for each probability. The average output powers were computed theoretically using (4) and empirically from the experimental output data within the main cluster. The results
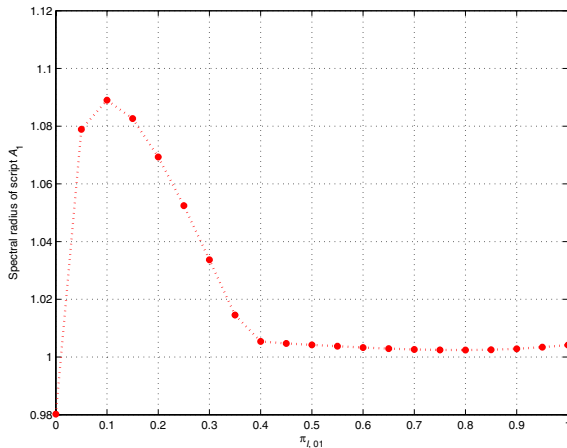
Fig. 7. The spectral radius of $\tilde{\mathscr{A}}_1$ as a function of $\pi_{I,01}$.
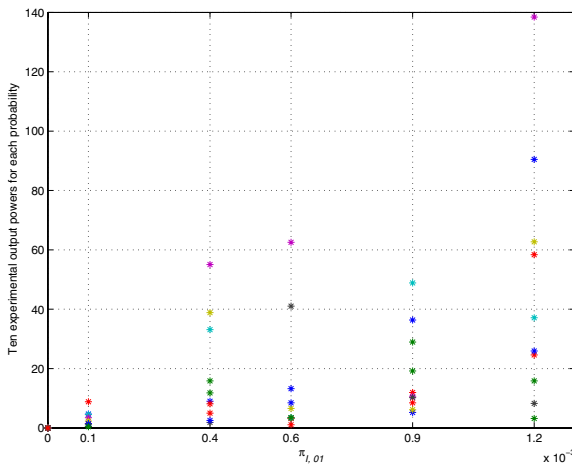
Fig. 8. The distribution of 10 output powers for six values of $\pi_{I,01}$.
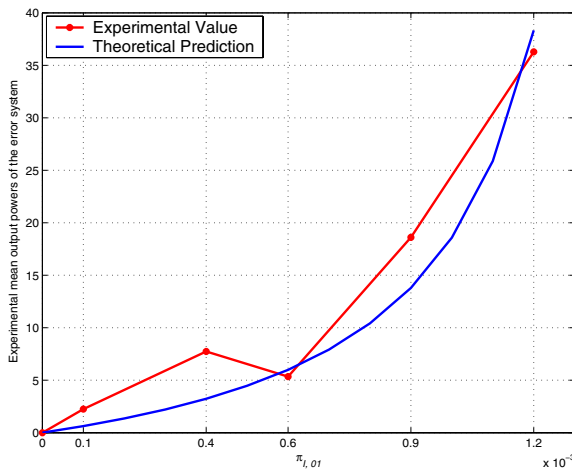
Fig. 9. The predicted mean output power in the tracking error as a function of $\pi_{I,01}$ and the experimental results for six values of $\pi_{I,01}$.

are shown in Fig. 9. In all cases, differences between the predicted average error powers and the experimental values

were small. Therefore, this error tracking model will be utilized in the future to analyze the data from the LANSCE experiment in order to better understand the effects of real neutron-induced rollback recoveries on aircraft tracking performance.

REFERENCES

[1] G. C. Messenger and M. S. Ash, *The Effects of Radiation on Electronic Systems*, 2nd ed. New York: Van Nostrand Reinhold, 1992.
[2] ——, *Single Event Phenomena*. New York: Chapman & Hall, 1997.
[3] E. Normand, "Single-event effects in avionics," *IEEE Trans. Nucl. Sci.*, vol. 43, no. 2, pp. 461–474, 1996.
[4] E. Normand and T. J. Baker, "Altitude and latitude variations in avionics SEU and atmospheric neutron flux," *IEEE Trans. Nucl. Sci.*, vol. 40, no. 6, pp. 1484–1490, 1993.
[5] R. Hess, "Computing platform architectures for robust operation in the presence of lightning and other electromagnetic threats," in *16th Digital Avionics Systems Conf. Proceedings*, Irvine, California, USA, 1997, pp. 4.3–9–16.
[6] ——, "Options for aircraft function preservation in the presence of lightning," in *Proc. 1999 International Conf. Lightning Static Electricity*, Toulouse, France, 1999, paper no. 106.
[7] R. Narasimhan, D. J. Rosenkrantz, and S. S. Ravi, "Early comparison and decision strategies for datapaths that recover from transient faults," *IEEE Trans. Circuits Syst.—I: Fundam. Theory Appl.*, vol. 44, no. 5, pp. 435–438, 1997.
[8] A. Ranganathan and S. J. Upadhyaya, "Performance evaluation of rollback-recovery techniques in computer programs," *IEEE Trans. Reliab.*, vol. 42, no. 2, pp. 220–226, 1993.
[9] W. S. Gray, H. Zhang, and O. R. González, "Closed-loop performance measures for flight controllers subject to neutron-induced upsets," in *Proc. 42nd IEEE Conf. Decision Control*, Maui, Hawaii, USA, 2003, pp. 2465–2470.
[10] S. Patilkulkarni, "Stability analysis of jump-linear systems driven by finite-state machines with Markovian inputs," Ph.D. dissertation, Department of Electrical and Computer Engineering, Old Dominion University, 2004.
[11] S. Patilkulkarni, H. Herencia-Zapana, W. S. Gray, and O. R. González, "On the stability of jump-linear systems driven by finite-state machines with Markovian inputs," in *Proc. 2004 Amer. Control Conf.*, Boston, Massachusetts, USA, 2004, pp. 2534–2539.
[12] O. L. V. Costa and R. P. Marques, "Mixed H_2/H_∞-control of discrete-time Markovian jump linear systems," *IEEE Trans. Automat. Contr.*, vol. 43, no. 1, pp. 95–100, 1998.
[13] ——, "Robust H_2-control for discrete-time Markovian jump linear systems," *Int. J. Control*, vol. 73, no. 1, pp. 11–21, 2000.
[14] O. L. V. Costa and M. D. Fragoso, "Stability results for discrete-time linear systems with Markovian jumping parameters," *J. Math. Anal. Appl.*, vol. 179, pp. 154–178, 1993.
[15] E. F. Hogge, "B–737 linear autoland Simulink model," NASA, Langley Research Center, Hampton, Virginia, USA, Tech. Rep. CR-2004-213021, 2004.
[16] M. Malekpour and W. Torres, "Characterization of a recoverable flight control computer system," in *Proc. 1999 IEEE Int. Conf. Contr. Appl.*, Kohala Coast-Island of Hawaii, Hawaii, USA, 1999, pp. 1519–1524.
[17] ——, "Characterization of a flight control computer with rollback recovery," in *19th Digital Avionics Systems Conf. Proceedings*, Philadelphia, Pennsylvania, USA, 2000, pp. 3.C.4–1–8.
[18] O. R. González, W. S. Gray, and A. Tejada, "Analytical tools for the design and verification of safety critical control systems," *2001 SAE Transact.—J. Aerosp.*, vol. 110, no. 1, pp. 481–490, 2002.
[19] A. Tejada, "Analysis of error recovery effects on digital flight control systems," Master's thesis, Department of Electrical and Computer Engineering, Old Dominion University, 2002.